

## 5. Experimental Results

Prototype models of the double spherical helix and the hemispherical helix studied in Sections 4.3.2 and 4.4 were constructed and measured. Fabrication of these antennas and measurement of their radiation patterns and axial-ratios are discussed in this chapter.

### 5.1 Fabrication of Prototype Spherical Helices

The double spherical helix was constructed using a styrofoam ball with a diameter (D) of 0.05 meter, while the 4.5-turn hemispherical helix is constructed using a ball of 0.04 meter in diameter. These balls only provide mechanical support for the antennas and have negligible effects on their radiation properties. A steel wire, 0.00019 meter in radius, is used to construct the sphero-helical windings. Also, a circular pan of 0.25 meters in diameter is chosen as a ground plane. With this ground plane, a minimum width of at least 0.5 wavelength at the lowest measurement frequency is maintained.

The construction of the double spherical helix and the 4.5-turn hemispherical helix began by first marking two directly opposite poles on each ball. The equator and four quadrature longitudinal lines in the directions of  $\theta = 0^\circ, 90^\circ, 180^\circ, \text{ and } 270^\circ$  were drawn on the sphere to ease defining the positions where the wire will pass through.

Since the spacing between the turns ( $S = \frac{D}{N}$ ) of the double spherical helix and the 4.5-turn hemispherical helix is constant, we can easily calculate the position along the z-axis corresponding to those longitudinal lines by using (3.2) for the double spherical helix and (3.5) for the 4.5-turn hemispherical helix. The positions along the z-axis of each longitudinal line were marked on a ruler that has the same length as the sphere's dimension and then projected onto its own longitudinal line. When the points were marked on the sphere, the steel wire was wound over the sphere by placing the wire adjacent to demarcated points on the longitudinal lines. Spray adhesive was applied to secure the wire to the sphere. Each constructed antenna was then soldered to a high performance and low RF leakage connector. Finally, the antenna assembly was mounted on a ground plane.

## 5.2 Measurement Results

Fabricated antennas were measured in the Virginia Tech Antenna Laboratory. The antenna range instrumentation is designed to operate over a wide frequency range, 1 GHz up to 30 GHz. Far-field pattern measurements for  $E_q$  and  $E_f$  components were carried out. Two sets of additional measurements in  $45^\circ$  and  $135^\circ$  planes were also performed in order to obtain axial ratios.

To achieve the desired plane cut for the radiation pattern, the source antenna was mounted on a positioner that can be rotated, thus allowing signals to radiate in various planes. The source antenna is connected to a generator whose frequency range and power level can be adjusted. The test antenna is connected to a receiver and a pattern recorder by means of a coaxial cable.

The measured radiation pattern data include amplitudes of  $E_q$  and  $E_f$  and their phases. Unfortunately, only the amplitudes of  $E_q$  and  $E_f$  are useable. This is due to the fact that, first, phases of  $E_q$  and  $E_f$  are very sensitive to distance. Secondly, these phases were obtained from the measurements at the end of the cable terminated into the receiver rather than at the test antenna terminals. For these reasons, the measured phase data are not reliable and not can be used in accurately determining the axial ratio.

### **5.2.1 Measurement of the Double Spherical Helix**

The double spherical helix was measured in the frequency range  $1.6 \text{ GHz} \leq f \leq 2.1 \text{ GHz}$ . With regard to the circular polarization performance of this antenna, as discussed in Section 4.5.1, the frequency  $f = 1.85 \text{ GHz}$  was used to compare the measured and calculated radiation patterns. Figures 5.1 (a) and (b) illustrate these patterns. It is emphasized that the  $E_q$  pattern in Figure 5.1 (b) is normalized to 0 dB, while the  $E_f$  pattern is normalized relative to the  $E_q$  pattern. The comparison of computed and measured results shows good agreement between radiation patterns. The magnitude of  $E_q$  is about 2 dB larger than that of  $E_f$  over the main beam. Several reasons may be stated for the difference between measured and calculated patterns, including deviation from precise spherical winding, environmental effects such as wind, reflections from surrounding objects and walls, and misalignment of source and test antennas.

### **5.2.2 Measurement of the 4.5-Turn Hemispherical Helix**

The hemispherical helix was measured over the frequency range  $2.6 \text{ GHz} \leq f \leq 3.5 \text{ GHz}$ . Figures 5.2 (a) and (b) show the computed and measured far-field patterns at a frequency of 2.8 GHz. It is seen from these figures that far-field patterns of the 4.5-turn hemispherical helix exhibit low backlobes and good symmetry.

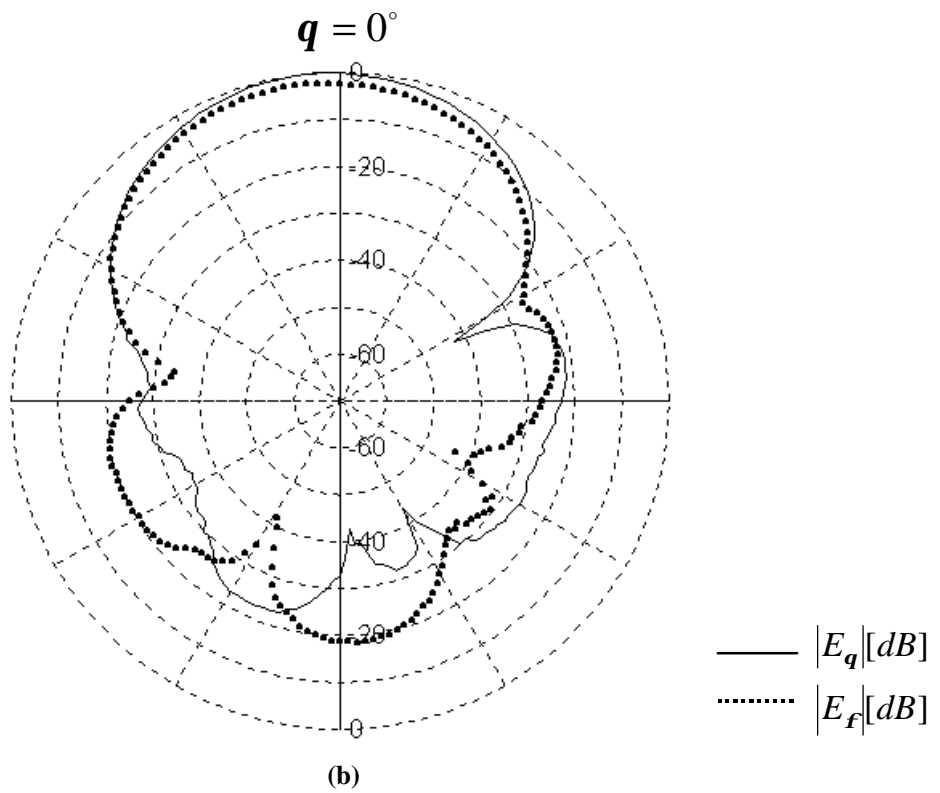
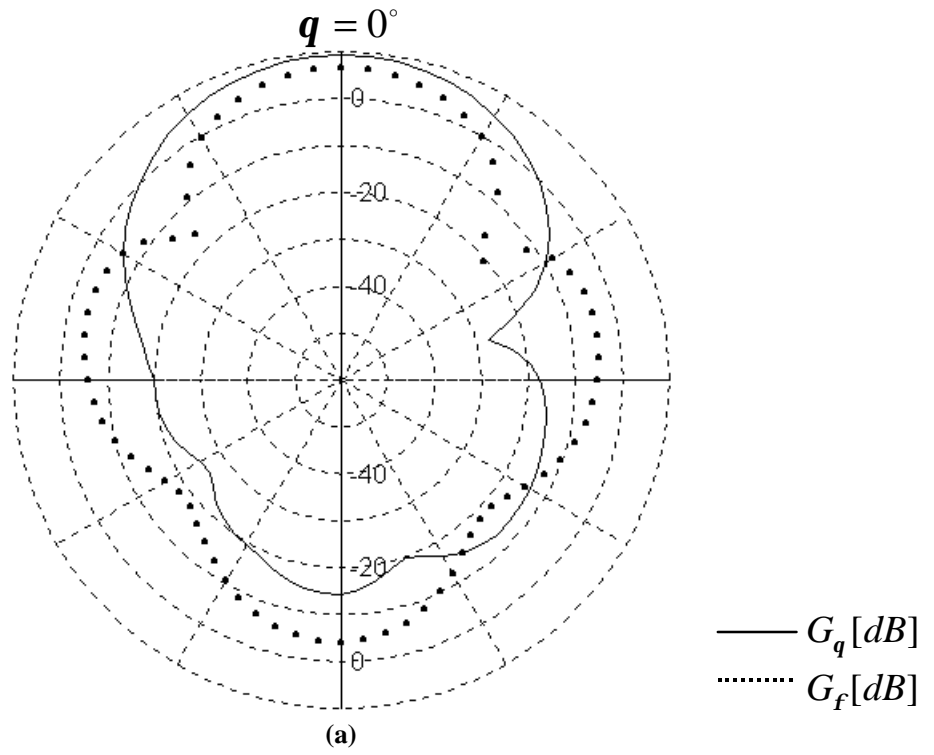


**Figure 5.1** (a) Computed and (b) measured radiation patterns for the double spherical helix at  $f = 1.85$  GHz.

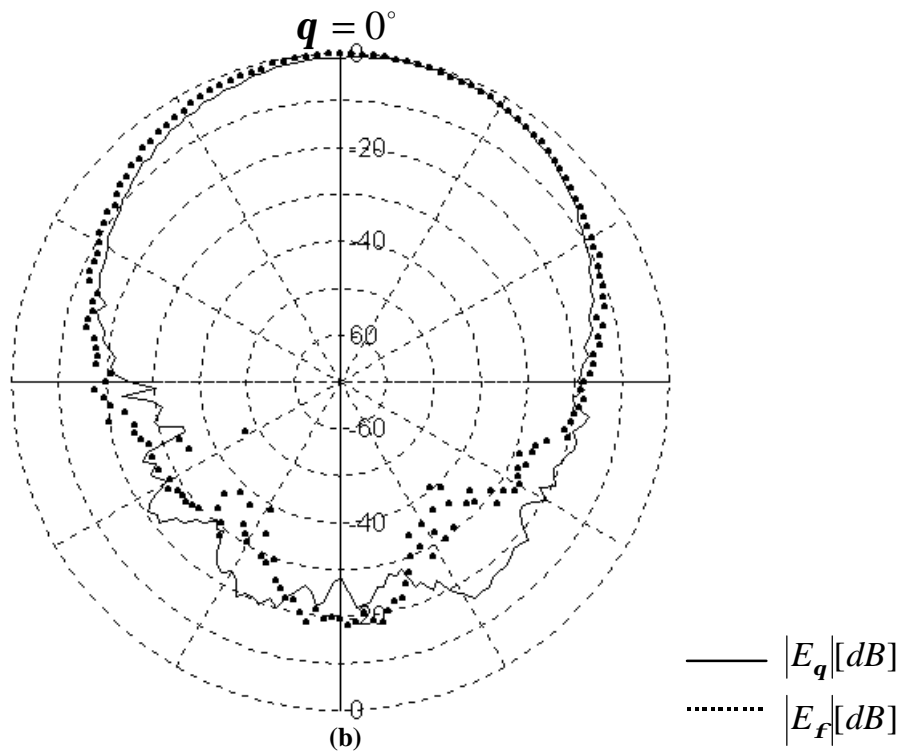
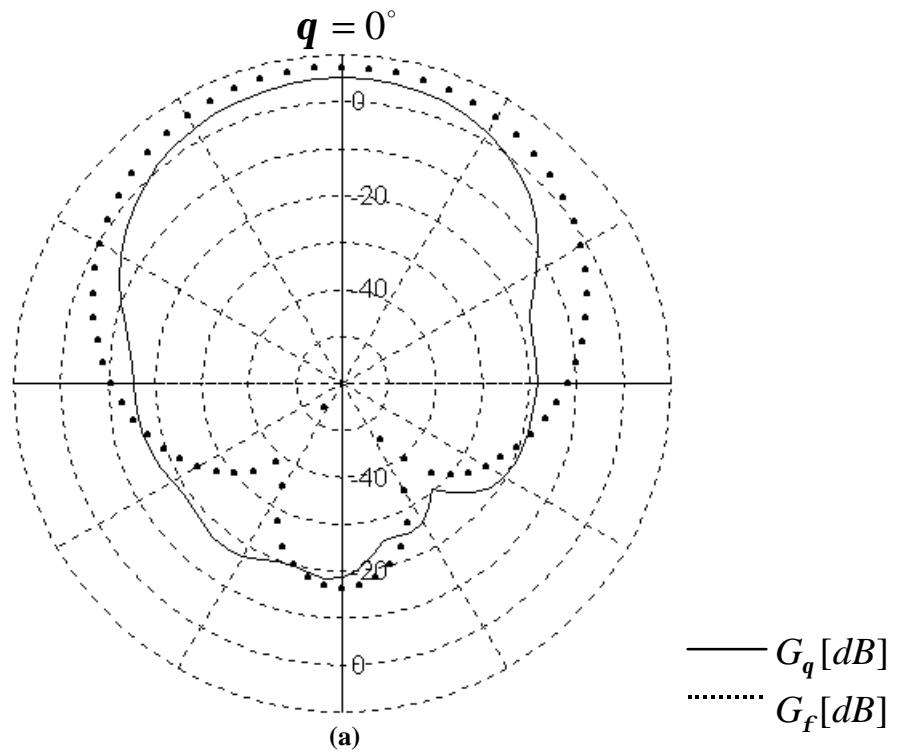


**Figure 5.2** (a) Computed and (b) measured far-field patterns for the hemispherical helix at  $f = 2.8$  GHz.

The backlobe level is generally 20 dB below the maximum peak. Moreover, this antenna provides a broad beamwidth over the entire frequency range. The 3-dB beamwidth of the 4.5-turn hemispherical helix over test frequencies is more than 60 degrees, while the 10-dB beamwidth is about 120 degrees. The calculated and measured patterns are in relatively good agreement. Radiation patterns at other frequencies are provided in Appendix D. Both numerical and experimental results signify that hemispherical helix is a promising broadbeam, circularly polarized, and narrow-band antenna.

### 5.3 Measurement of Axial Ratio

Since the measured phases of  $\mathbf{q}$  and  $\mathbf{f}$  components of fields are not reliable, the axial ratio is determined using a technique based on multiple amplitude components [19]. To use this technique, additional measurements of  $E_q$  and  $E_f$  components in  $45^\circ$  and  $135^\circ$  directions are required. The axial ratios calculated from this method are shown in Figure 5.3. Comparison of Figures 4.19 and 5.3 indicates that predicted and measured axial ratios are in reasonably good agreement. The lowest measured axial ratio occurs at  $f = 2.85$  GHz and is about 2 dB.

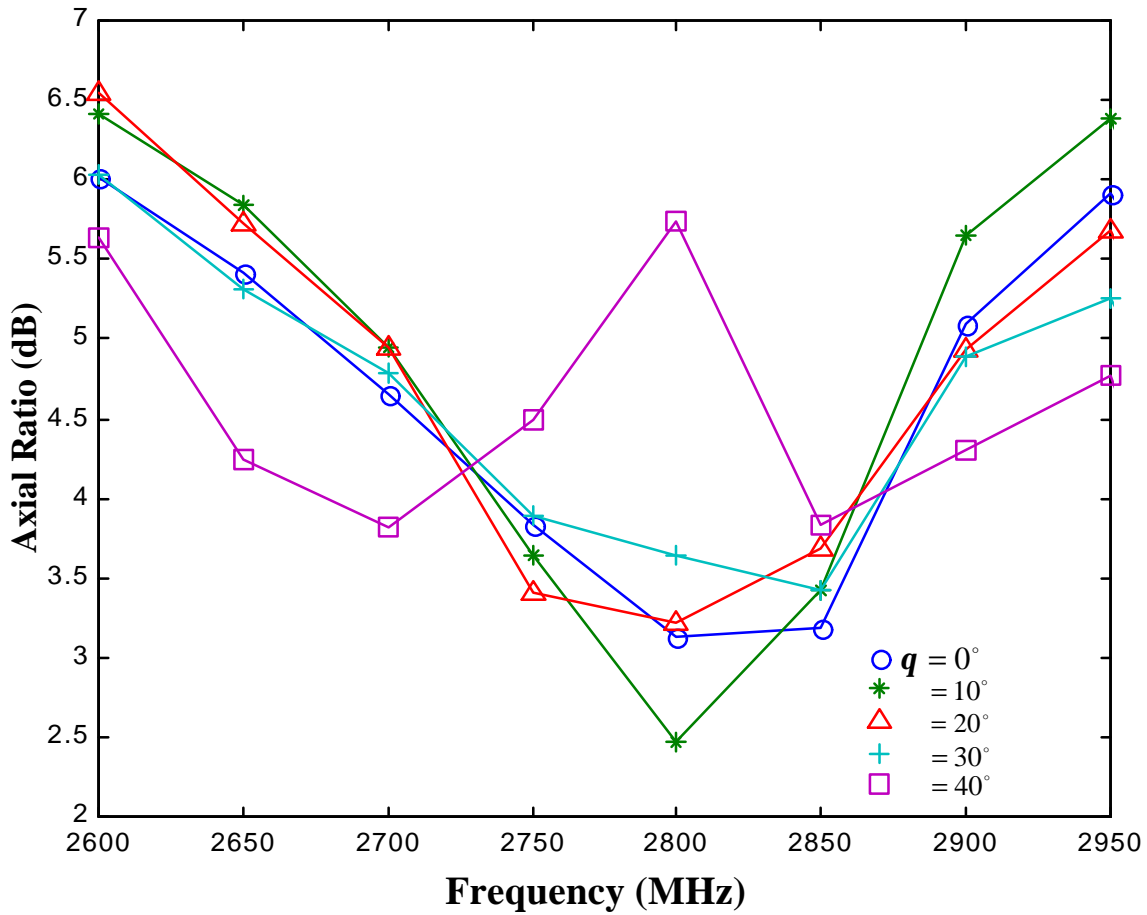


Figure 5.3 Computed axial ratio from measured pattern data for the 4.5-turn hemispherical helix.